Geological Field Trips and Maps



# UAV-based high-resolution mapping of a complex landslide: an example from Basilicata, southern Italy

https://doi.org/10.3301/GFT.2023.01

2023
Vol. 15 (1.1)

ISSN: 2038-4947

**GFT&M** - *Geological Field Trips and Maps*

Periodico semestrale del Servizio Geologico d'Italia - ISPRA e della Società Geologica Italiana
Geol. F. Trips Maps, Vol.**15** No.1.1 (2023), 14 pp., 7 figs., 1 tab., (https://doi.org/10.3301/GFT.2023.01)

# UAV-based high-resolution mapping of a complex landslide: an example from Basilicata, southern Italy

**Paolo Giannandrea[1], Massimo Bavusi[2], Lucia Contillo[1], Donato Lacava[2], Salvatore Laurita[2], Marcello Schiattarella[1]**

[1] Dipartimento delle Culture Europee e del Mediterraneo, Università della Basilicata, via Lanera, 20 – 75100 Matera
[2] TERRALAB s.r.l., viale del Basento, 118 -85100 Potenza

Corresponding Author e-mail address: paolo.giannandrea@unibas.it



**Cover page Figure**
...

ISSN: 2038-4947 [online]

http://gftm.socgeol.it/

*INDEX*

**Introduction** ..... 4

**Methods and techniques** ..... 4

Flight methodology ..... 4

Geological and geomorphological mapping ..... 5

**Contents description** ..... 7

**Discussion and conclusions** ..... 13

**References** ..... 14

## ABSTRACT

This paper accompanies a UAV-based geological-geomorphological map (1:1,000 scale) of a complex landslide periodically re-activated, localized not far from the town of Potenza in Basilicata, southern Italy. A fixed-wings eBee drone equipped with a conventional digital RGB photocamera (*senseFly* S.O.D.A.) was used to collect airborne digital elevation models (DEMs), orthophotos, and density point clouds in 2014 and 2018. The two photogrammetric surveys helped us to quickly detect the features of the new mass movement episodes. Three Google Earth Pro orthophotos filled the lack of information of the years in between. Topographic contours of the landslides with their morphological scarps and geological data from the 2018 field survey were processed using free and open-source software QGIS 3.22.4. For graphic adjustment and the final layout, the main map was imported into Adobe Illustrator CC 2018 and CorelDraw and embedded into an A0 map frame.
The geological-geomorphological map reports a detailed representation of the bedrock geological structures, the ancient landslide bodies now stabilized, and the recent landslides occurred from 2014 to 2018 as deduced by the multitemporal analysis. Geomorphic features and facies analysis allowed us to interpret as debris flows and mud flows the depositional processes responsible for the genesis of the landslide bodies reaching the thalweg of the Basento River.

*Keywords:* Unmanned Aerial Vehicle (UAV), debris and mud flows, landslide mapping, Basento River, southern Apennines (Italy).

## INTRODUCTION

The study area is located in the southern Apennines, on the left side of the Basento River valley not far from the village of Brindisi di Montagna (Fig. 1). In this sector an about 800 m-long active landslide, labelled "*colata di Brindisi di Montagna scalo*" (hereafter **BML**) is present (Cotecchia et al., 1986; Bentivenga et al., 2006) and occupies most part of the slope. It is a multi-temporal earth flow (period of activity: from 1973 to 2016; Cotecchia et al., 1986; Bentivenga et al., 2019) classified by Cotecchia et al. (1986) and Bentivenga et al. (2006) as a "rotational slide-flow" (Cruden and Varnes, 1986). The moving materials detach from the *Flysch Rosso* formation starting from a toe of an existing landslide terrace and deposited within a channel above the *Gruppo delle Argille Variegate* (Spilotro et al., 2016).
The geological map of the study area was published at 1:50,000 scale on the official map (sheet n. 470 "Potenza" - Servizio Geologico d'Italia, 2012) and as a sketch map in the papers by Cotecchia et al. (1986) and by Bentivenga et al. (2006, 2019). All these maps show a similar geological bedrock made up of Flysch Rosso, cropping out in the feeding area of the landslide, and of the Gruppo delle Argille Variegate, outcropping in the accumulation area along the Basento River. The two lithostratigraphic units are separated by a NW-SE-striking fault. The mapping of Quaternary deposits was carried out by those authors through the stereoscopic observation of IGM (Istituto Geografico Militare) aerial photos, integrated with field-survey controls. No information about the type of topographic support used for the mapping is given. Geological data from the sheet n. 470 Potenza have been processed using an outdated topographic map. It is worth noting that in the areas affected by earth-flow landslides each mass movement produces accumulation bodies that modify the topography. Therefore, a perfect restitution of post-event modified topography is necessary for a correct multi-stage landslide geological mapping.
For multitemporal landslide detection, such as Digital Image Correlation, more techniques have been developed in recent years (e.g., Turner er al, 2015; Stumpf et al,. 2017; Mazzanti et al., 2020; Guerriero et al., 2020). In our work we used a 1:1,000 scale map processed from UAV-based remote sensing of a 2018 flight. The UAV-based landslide monitoring is a viable method (Turner et al., 2015) to provide an efficient, low-cost, and rapid framework for the survey of active slopes (Clapuyt et al., 2016). Our study is based on a detailed stratigraphic analysis of both the sedimentary bedrock and the Quaternary cover units. These latter, largely consisting of landslide deposits, have been classified as informal units bounded by unconformities.

## METHODS AND TECHNIQUES

### Flight methodology

The first stage of the workflow consists in the definition of an *ad hoc* flight plan, to ensure the best coverage of the target area, with an optimal photo overlap in frontal (overlap) and lateral direction (sidelap), taking into account the camera footprint at a certain altitude. The drone used for this case study is an eBee with a fixed wing from *sensefly* Parrot Group. The eBee allowed us to map a large area in a single automated mapping flight at low altitude and acquire images with high resolution (4 cm/pixel). We chose this resolution to get the best possible detail. We knew that the software *sensefly* eMotion, that controls the drone during flight, could use digital elevation data to support such a flight planning and keep the drone's altitude consistent above the terrain.
In terms of images overlap, we chose 75% lateral and 60% longitudinal overlaps, in order to guarantee a sufficiently redundant coverage of the studied area, using a S.O.D.A._10.6_5472x3648 (RGB) camera. Digital photogrammetry, based on the concept of stereoscopic photogrammetry, allows the reconstruction of a 3D

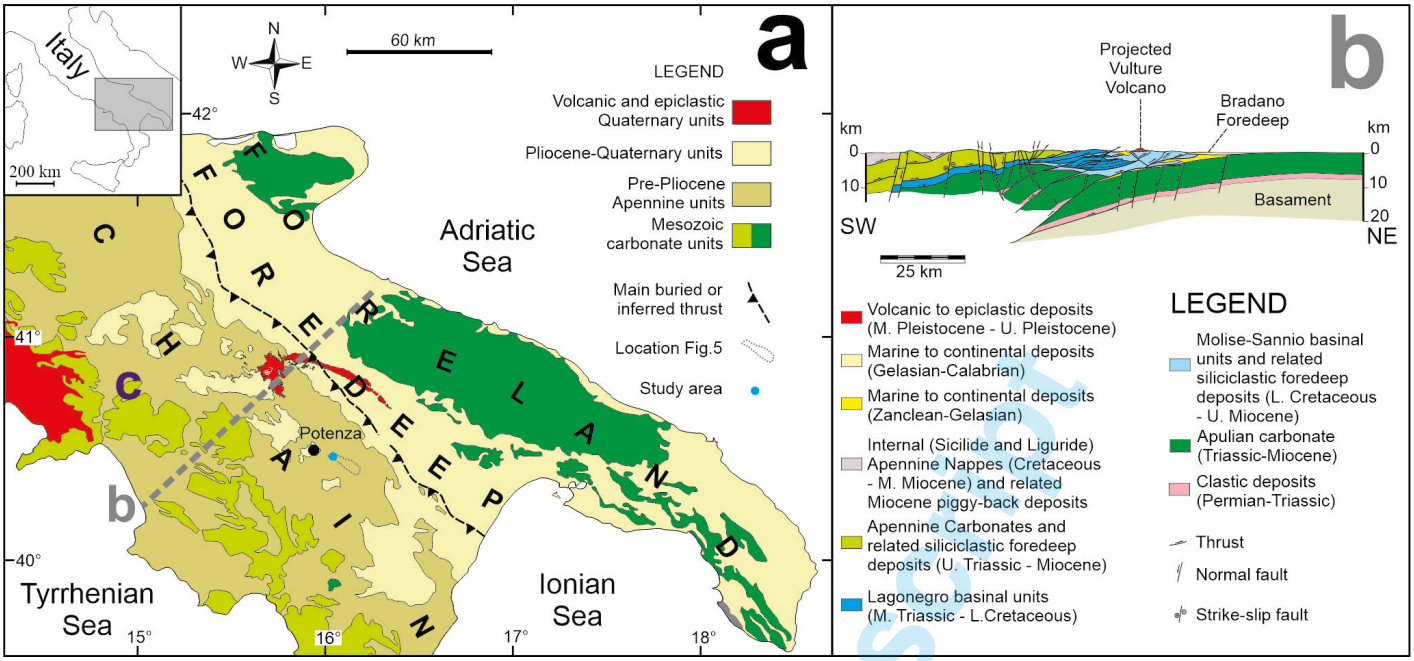


**Fig. 1 - a) Regional geological framework with locations of the study area and the area of figure 6; b) Regional geological cross-section (modified after Scrocca, 2010).**

topographic surface model by triangulating the position in the 3D space of pixels that are visible in two or more images. Once images are oriented and, possibly, calibrated, it is possible to derive DSM (Digital Surface Model) and orthophotos along with very high-definition point clouds. Following each flight, a total of 545 captured images were processed using the Pix 4D software. Pix4D mapper is advanced photogrammetry computer algorithms that automatically processes the images that were taken from the air using unmanned aircraft, or from the ground with a digital camera. It uses technology that works on the principle of recognizing the image content (pixels) to make a complete 3D model (e.g., point clouds, digital surface model and terrain model, orthomosaic and contour lines). Pix4D allows to generate a DSM or a DTM (digital terrain model) and high-resolution orthomosaic with a known ground sampling distance (GSD) of 20 cm per pixel. For ground control of the generated 3D models, a significant number of points (GCPs) are then collected using an RTK-GPS based on objects on the ground that can be easily recognized in the aerial photos with a homogeneous spatial distribution on the scene. The images have been processed and implemented in a GIS environment using QGIS package.

## Geological and geomorphological mapping

Two high-resolution orthomosaic images assembled by means of the flight missions carried out in 2014 and 2018 (Fig. 2) were used to investigate the active slope area of the **BML**: more multistage landslide bodies and geomorphological features have been recognized and transferred on a 1:1,000 scale topographic base map processed in 2018 and into two 3D digital modelled surfaces (a DSM from the 2014 survey and DTM from the 2018 survey; Fig. 2). Coordinates frame of the map is expressed in WGS 1984 UTM Zone 33N (EPSG:32633) and indicated at the margins of the map sheet. In addition, to distinguish the events that occurred before 2014 and between the years 2014 and 2018, Google Earth Pro orthophotos were used (Fig. 3). The field work made it possible to perform the stratigraphic reconstructions of both the sedimentary bedrock (Fig. 4a) and the landslide deposits (Fig. 4b), reported in the attached map at 1;1,000 scale. Lithological descriptions and facies analysis of the landslide materials were used for the interpretation of mass movement processes.

In agreement with the papers by Sabato et al. (2007) and Giannandrea et al. (2016) related to the territory closely east of the study area (i.e., around the Albano di Lucania, Campomaggiore, Pietrapertosa, and Castelmezzano villages), we used lithostratigraphic criteria for the nomenclature of the Sicilide and Lagonegrese units, and synthem stratigraphy criteria (Chang, 1975) for the Irpinian units (largely consisting of *flysch di Gorgoglione*). It is well-known that the basic unit of the lithostratigraphy is the formation, that divides a body of rock form the others in relation to a suit of age and lithologic characteristics (Hedberg, 1976), whereas Unconformity Bounded Stratigraphic Units (UBSU) define rock volumes (synthems, grouped in supersynthems and divided in subsynthem) bounded by significant unconformities (Salvador, 1987, 1994). Finally, for landslide mapping we adopted the

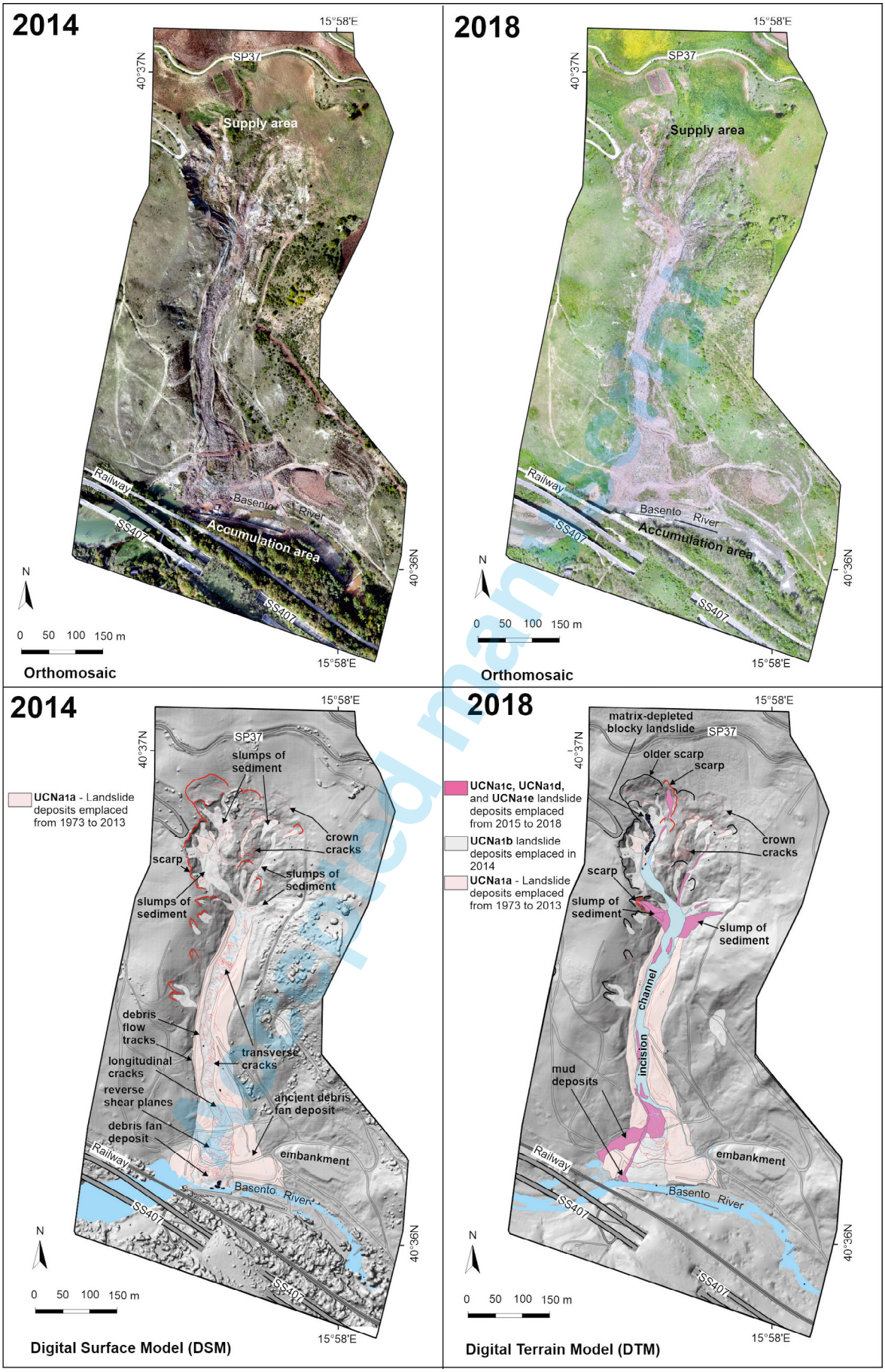


**Fig. 2 - 2014-2018 orthomosaics and 2014-DSM and 2018-DTM images of the study area with the geomorphological features of the BML.**

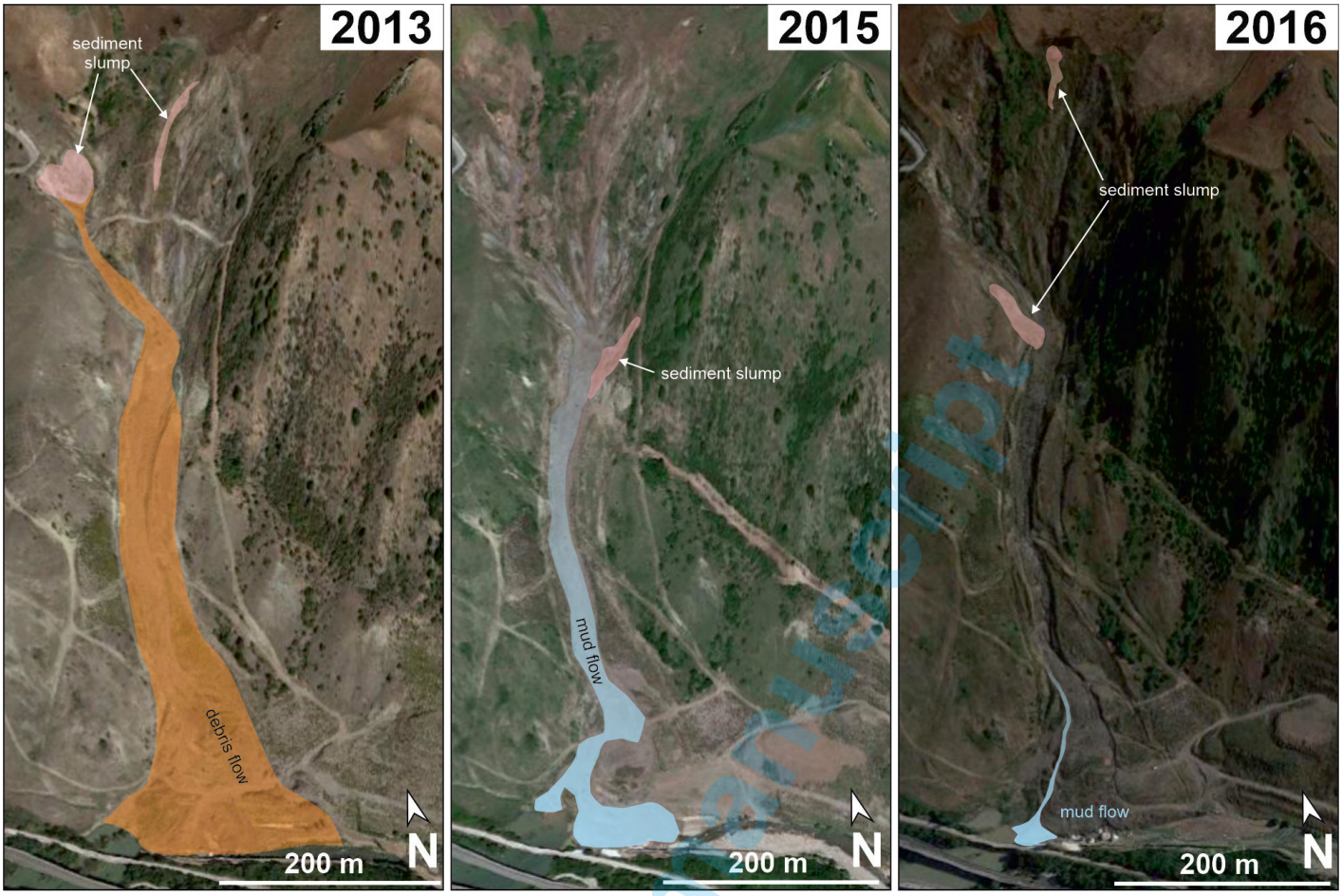


**Fig. 3 - 2013, 2015, and 2016 Google Earth Pro orthophotos of the study area showing the landslide deposits emplaced in the reference year.**

allostratigraphic criteria (NACSN, 1983), that identify sedimentary bodies on the basis of their relations with bounding discontinuities, including geomorphic surfaces.
Our stratigraphic model (Fig. 4b) allows distinguishing different superposed discontinuity-bounded deposits which display similar lithology. The stratigraphic correlations between the study area and its surroundings were carried out based on a wider (i.e., 1:10,000 scale mapping) geological field survey (Fig. 5).

## CONTENTS DESCRIPTION

The map area of the active multistage BML and its surroundings includes a 0.5 km-wide and 1.10 km-long territory developed between the altitudes of 700 and 500 m a.s.l. on the left side of the Basento River, in front of the Brindisi di Montagna village on the opposite side. This map displays i) several landslide deposits organized according to the stratigraphic position, ii) the bedrock units involved in the landslide processes, iii) colluvial (locally anthropically reworked) and present-day alluvial deposits, iv) ridges and embankment created for motorway/railway and by accumulation of earth excavated from landslides.
The bedrock consists of clay, limestone, and sandstone, ranging in age from the Cretaceous to the Miocene, related to deep basinal or foredeep units (Lagonegro, Sicilide, and Irpinian); lithological descriptions, in the same stacking order as the legend in figure 5, are reported in table 1.
The Lagonegro Units cropping out along the left side of the Basento River and around the Trivigno village (Fig. 5) are represented by the Campomaggiore, *Flysch Rosso*, *Paola Doce*, and *flysch numidico* formations: in the area of the BML map, only those of Campomaggiore and *Flysch Rosso* are present, dipping counterslope at the highest altitudes of the study area (see a-a' cross-section in the attached geological-geomorphological map). The geometric position of such formations retraces the original stratigraphic relationships, but their contact is here sheared. The *Campomaggiore formation*, late Valanginian - early-middle Albian in age (Sabato et al., 2007), was subdivided into the $CAM_1$, $CAM_2$, $CAM_3$, and $CAM_4$ lithofacies: $CAM_1$ (Fig. 6a) and $CAM_2$ (Fig. 6b) consist of very deformed layers with a prevalent clayey composition, whereas $CAM_3$ (Fig. 6c) and $CAM_4$ (Fig. 6d) show thin parallel layers made up of clay

**Tab. 1 - Lithological descriptions of the bedrock units after Sabato et al. (2007), Giannandrea et al. (2016), and Schiattarella et al. (2016).**

| Stratigraphic units of the bedrock | | | | | | | | |
|---|---|---|---|---|---|---|---|---|
| **Palaeogeographic unitsa** | | **supersynthem** | **synthem** | **subsynthem** | **Units code** | **Description of lithology and deposits interpretation** | **Thick (m)** | **Biostratigraphic age** |
| Irpine | | Gorgoglione | | | 8 | Conglomerate and sandstone not included in synthems. | 200 | |
| | | | Castelmezzano | | 8d2 | Thin beds of fine-grained, horizontal and cross-stratified thinly laminated silty sandstones with isolated lenses-shaped metric intercalations of chaotic pelite beds, and pebbly sandstones (turbidite deposits). In the 400 m thick upper portion high lateral continuity tabular bed-set, about 1-5 m thick, of contourite deposit are present. | 1550 | Langhian-Tortonian Zones MNN5b- MNN11b at the top MMi7a (Giannandrea et al., 2016) |
| | | | | | 8d1 | Amalgamated metric beds of coarse-grained, massive sandstones, with intercalations of middle-grained, thin horizontally laminated sandstone (turbidite deposits). | | |
| | | | Cirigliano | Pietra del Corvo | 8c2 | Fining- and thinning-upward muddy sandstones (turbidite deposits). | 500 | Langhian Zones MNN4b?- MNN5a (Giannandrea et al., 2016) |
| | | | | | 8c1 | Thick pebbly sandstones amalgamated beds, organized in sequence 9 - 35 m thick. At the top of each sequence 1-2 m thick of coarse- to fine-grained, horizontal to large- to medium-scale cross stratified sandstone is present (turbidite deposits). | | |
| | | | | Pozzo del Pellegrino | 8b | Thinning-upward fine-grained sandstones and mudstones in thin alternating beds (turbidite deposits). | ~100 | Burdigalian-Langhian transition Zone MNN4b (Giannandrea et al., 2016) |
| | | | | Ponte della Vecchia | 8a | Amalgamated beds (0.50-6 m tick) of coarse-grained sandstones and conglomerates, with, in the uppermost 10 m thick part, rare intercalation of middle-grained, thin horizontally laminated sandstone (turbidite deposits). | 100 | Burdigalian-Langhian transition Zone MNN4a (Giannandrea et al., 2016) |
| | group | formation | | member | | | | |
| Irpine | | Val Miletta | | chaotic varicoulored clays | 7d | Chaotic varicolored clays, with blocks (some ten meters size) of calcarenite and quartzarenites (olistostrome). | From some meters to a few hundred meters | |
| | | | | silty clay sandstones | 7c | Thin alternation of silty clays and massive and laminated middle-to fine-grained turbiditic sandstones. | 50-60 | |
| | | | | quartzarenites | 7b | Amalgamated beds of quartzarenites | 25 | |
| | | | | green quartzose sandstones and calcareous marls | 7a | Middle-to fine-grained, graded sandstone beds and silt, marls and thin-laminated marly clay with intercalations of fine-grained calcarenite (turbidite deposits and pelagic sediments). | 25 | |
| Lagonegrese | | flysch numidico | | quartzarenites | 6 | Coarse-grained quartzarenite, organized in 8-9 m thick banks and 30 to 80 cm thick beds, with decimetric interbedded layers of clayey marls (turbidite deposits). | Max 300 | Early Miocene (Schiattarella et al., 2016) |
| | | Paola Doce | | calcareous marls | 5 | Medium- and fine-grained calcarenite with intercalations of marly limestone, marls and calcisiltite in 10 to 40 cm thick beds. | 475 | late Oligocene – Early Miocene (Schiattarella et al., 2016) |
| | | Flysch Rosso | | calcareous marls | 4b | Grey, brown, and red laminated marly clay, with intercalations of both massive and graded calcarenite in decimetric beds (pelagic and turbidite deposits). | | Early Cretaceous – Oligocene *p.p.* (Pescatore et al., 1999; Scandone, 1972) |
| | | | | cherty | 4a | 1 to 10 cm thick beds of black and red chert, with frequent intercalations of brownish and red marly clay (pelagic sediments). | 10 | Albian – early Turonian (Sabato et al., 2007) |
| | | Campomaggiore | | siliceous claystone | 3 | Thin laminated dark grey-green siliceous claystone with subordinate red beds of siliceous radiolarian mudstone and rare cm-beds of black shales and fine-grained calcarenite and calcilutite (pelagic sediments and subordinate turbidite). | ~200 | late Valanginian - early-middle Albian (Sabato et al., 2007) |
| Sicilide | | Corleto Perticara | | calcareous marls | 2 | Alternation of marly clay, marly limestone calcareous marls, and yellowish gray calcilutites with subordinate beds of calacarentite (pelagic sediments and subordinate turbidite). | Max 250 | Eocene – Early Miocene |
| | Argille Variegate | | | varicoloured clays | 1 | Red, green, and grey clay and marly clay, with a chaotic attitude and/or affected by intense deformation (pelagic deposits). | Few hundreds | Cretaceous – Early Miocene (Schiattarella et al., 2016) |

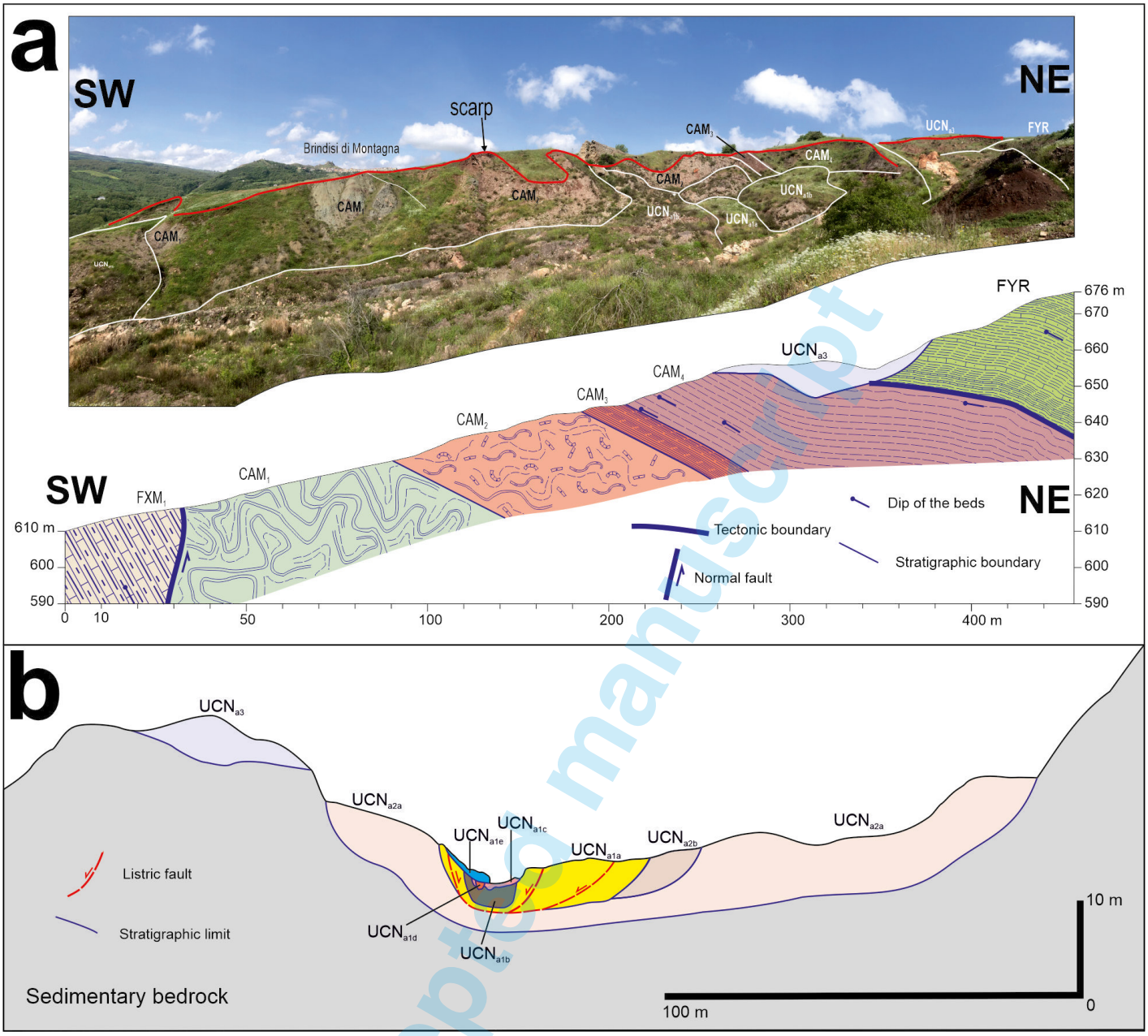


**Fig. 4 - a) Panoramic view and a-a' geological cross-section reported in the map to illustrate the relationships of the bedrock units in the landslide source area; b) landslide stratigraphic scheme in an ideal transverse section.**

with rare intercalations of calcarenite and black shales. The *Flysch Rosso* consists of alternate beds (5-30 cm thick) of marly clay and calcarenite (Fig. 6e; age: Early Cretaceous p.p. – Oligocene?; Pescatore et al., 1999; Scandone, 1972). The Irpinian Units crop out at Brindisi di Montagna and on both sides of the Basento River between Trivigno and Campomaggiore villages. These units include turbidite deposits related to different geological formations, partly coeval but different for palaeogeographical pertinence and/or source area (Pescatore et al., 1971; Cocco et al., 1972; Pescatore, 1978; Patacca et al.,1990). In the investigated sector (Fig. 5), only the *flysch di Gorgoglione* crops out. This succession conformably lies on the flysch numidico and shows four internal unconformities reflecting the deformation of the fold-and-thrust belt of the South Apennine orogenic wedge (Giannandrea et al., 2016). The unconformities recognized between the Castelmezzano and Accettura villages have been used by Giannandrea et al. (2016) for the stratigraphic subdivision of the succession into the Val Miletta formation and Gorgoglione supersynthem (Fig. 5). The lowermost Val Miletta formation includes several lithofacies made of Numidian-like quartzarenite, Gorgoglione-like fine-grained turbidite sandstones, and, at the top, chaotic deposits of varicoloured clays, with mega-block of calcarenites and calcareous marls. The Gorgoglione supersynthem is subdivided into the Cirigliano (grouping the Ponte della Vecchia, Pozzo del Pellegrino, and Pietra del Corvo subsynthems) and Castelmezzano synthems.

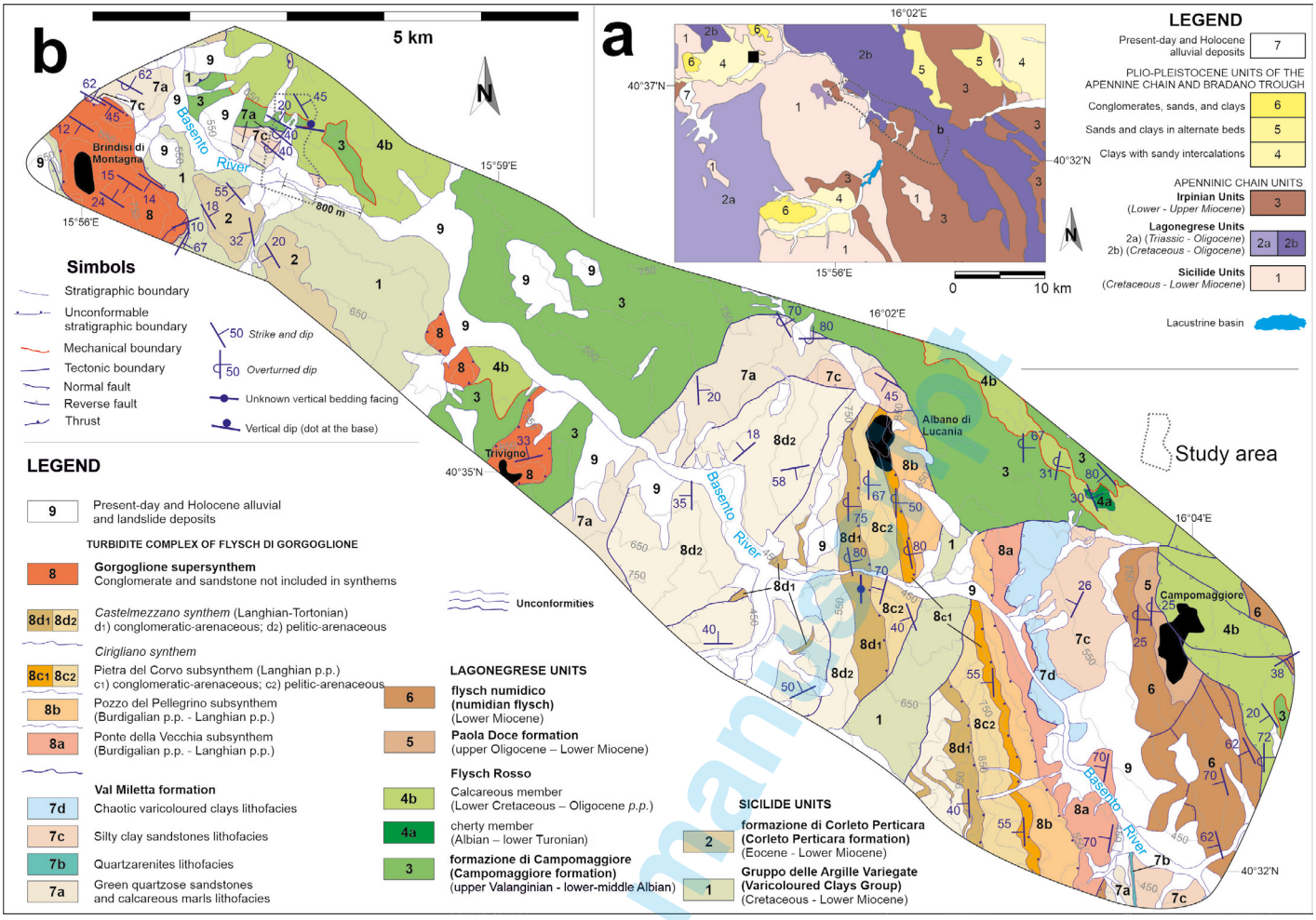


**Fig. 5 - a) Geological scheme of a portion of south-Apennine chain and b) geological map of the Lucanian Apennine along the Basento River between Brindisi di Montagna and Campomaggiore (location in Fig. 1a).**

The three subsynthems are fining- and thinning-upward turbidite successions, with conglomerate alternated to coarse-grained sandstone at the base and mudstone with thin beds of fine-grained sandstone at the top. The Castelmezzano synthem includes two vertical lithofacies (code 8d1 e 8d2 in Fig. 5). The lithofacies 8d1 consists of amalgamate beds of coarse-grained turbidite sandstones with pebbles, whereas the lithofacies 8d2 is made of sandy mudstones with isolated metric lens-shaped intercalations of pebbly sandstones.

In the central portion of the attached map silty clay lithofacies with intercalations of both laminated calcilutite and calcarenite (Fig. 6f; $FXM_1$) and of medium to coarse-grained sandstone (Fig. 6g; $FXM_2$) of the Val Miletta formation crop out.

The Sicilide Units were mapped on the right side of the Basento River in the north-western sector of the map reported in figure 5. Among this units, only the clayey broken formation of the *Gruppo delle Argille Variegate* (Cretaceous - Lower Miocene; Schiattarella et al., 2016) is present at the edges of the thalweg of the Basento River.

The units described above are bounded by two NW-SE-directed faults which form a staircase from the elevation of 700 m a.s.l. to the thalweg of the Basento River. The scissor fault that bounds the Lagonegro and Irpinian units is displaced by a N-S-trending right-lateral strike-slip fault, located under the landslide deposit, longitudinally to the channel.

The detailed field survey of the BML allowed us to distinguish two other groups of landslides ($UCN_{a2}$ and $UCN_{a3}$) stratigraphically underlying the active landslide. The oldest $UCN_{a3}$ landslide crops out at highest elevation (between 630 and 700 m a.s.l.) and shows the morphological relicts of the oldest landslide scarps. It consists of structureless reddish gravelly silty clay interpreted as debris flow deposits (facies $x_1$, Fig. 7), with carbonate angular clasts ranging in size from 4 to 50 cm. The $UCN_{a2}$ extends from about 650 m a.s.l. to the thalweg of the Basento River where it crops out for about 800 m with the facies $x_1$ (Fig. 5). In the accumulation area, a surface separates the unit into the $UCN_{a2b}$ and $UCN_{a2a}$ bodies. The absence of the grey and green clay inside the facies $x_1$ suggests a source area just

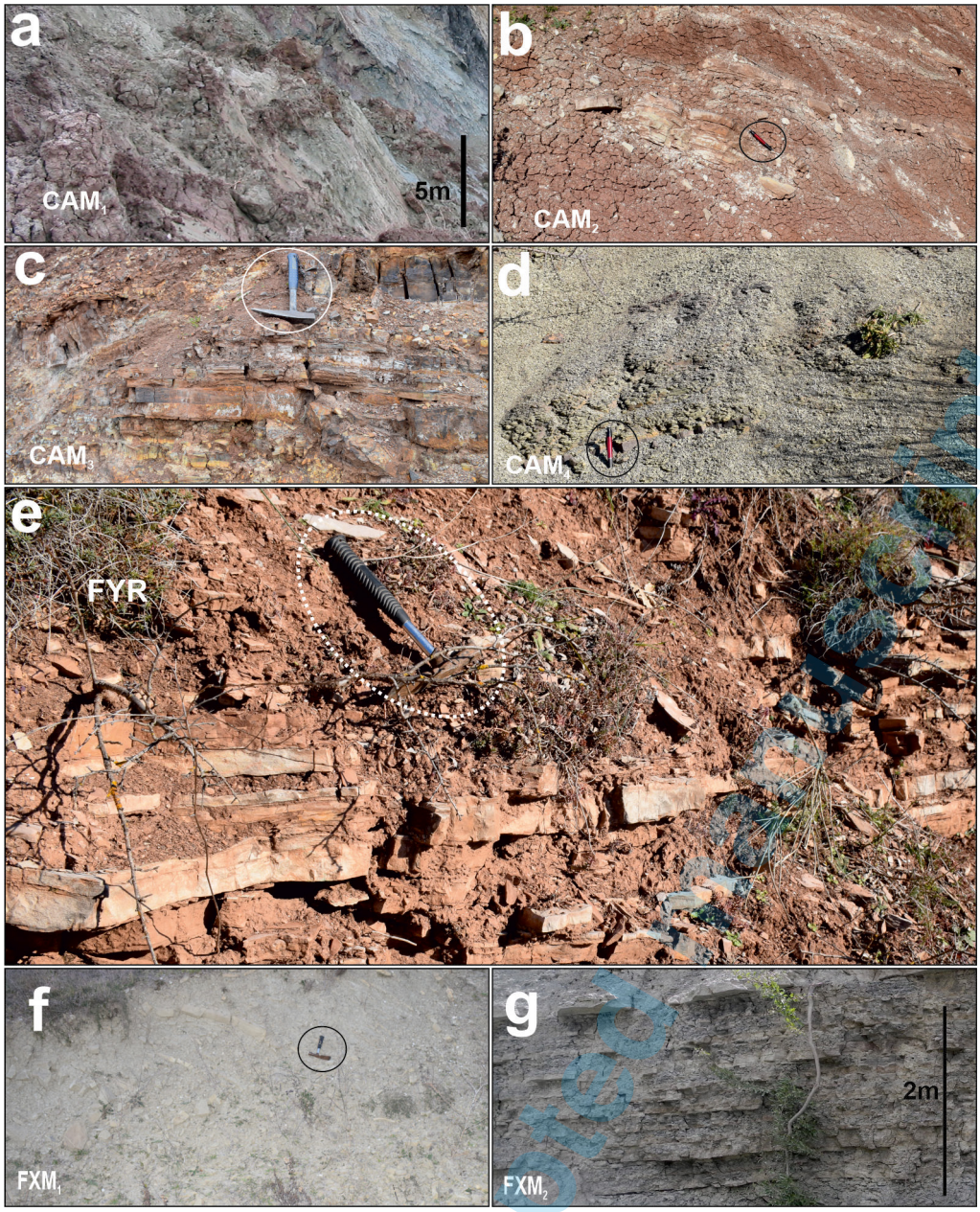


**Fig. 6 - Pictures showing bedrock lithological characters of: a to d) Campomaggiore formation, e) *Flysch Rosso* , and f and g) Val Miletta formation; for lithology descriptions see text.**

from the highest portion of the studied area, where the *Flysch Rosso* and the UCNa3 landslide crop out.

The active BML, identified in the map with code $UCN_{a1}$, fills a second U-shaped channel cutting both the Campomaggiore formation and the $UCN_{a2}$ landslides. It is subdivided into the 1973 to 2013 $UCN_{a1a}$ and other four groups of landslide bodies (from the $UCN_{a1b}$ to the $UCN_{a1e}$). Each group, related to the years 2014, 2015, 2016, and 2017-2018, respectively assembles several landslide bodies with different facies and geomorphological features. The $UCN_{a1a}$ unit includes several landslide bodies made of debris flow deposits (facies $x_2$), extended along the BML channel from the source area to the accumulation zone, and four landslide bodies made of sediment slump in the source area (facies z). The landslide deposit with facies z extends for a few hundred square meters below its main scarp and present internal fractures. Along the BML channel the landslide $UCN_{a1ax2}$ shows several lateral slip secondary scarps with a longitudinal channel trend. The facies $x_2$ (Fig. 7) consists of structureless red, grey, and green clay with carbonate angular clasts and blocks ranging in size from 4 cm to 1-2 m. The colour of the clay suggests for this group of landslides a source rock mainly represented by the Campomaggiore formation and subordinately by the *Flysch Rosso* and ancient landslide $UCNa_3$. The facies z (Fig. 7) consists of very deformed grey-green and red clay with isolated calcareous clasts. For each landslide included in the $UCN_{a1b}$-$UCN_{a1e}$ units, the orthophotos allowed us to define the geomorphological characteristics such as scarp, shape, and extension of the landslide deposit. The $UCN_{a1b}$ unit (year 2014) groups a debris flow deposit (facies $x_2$) located along the BML channel from the source area to the

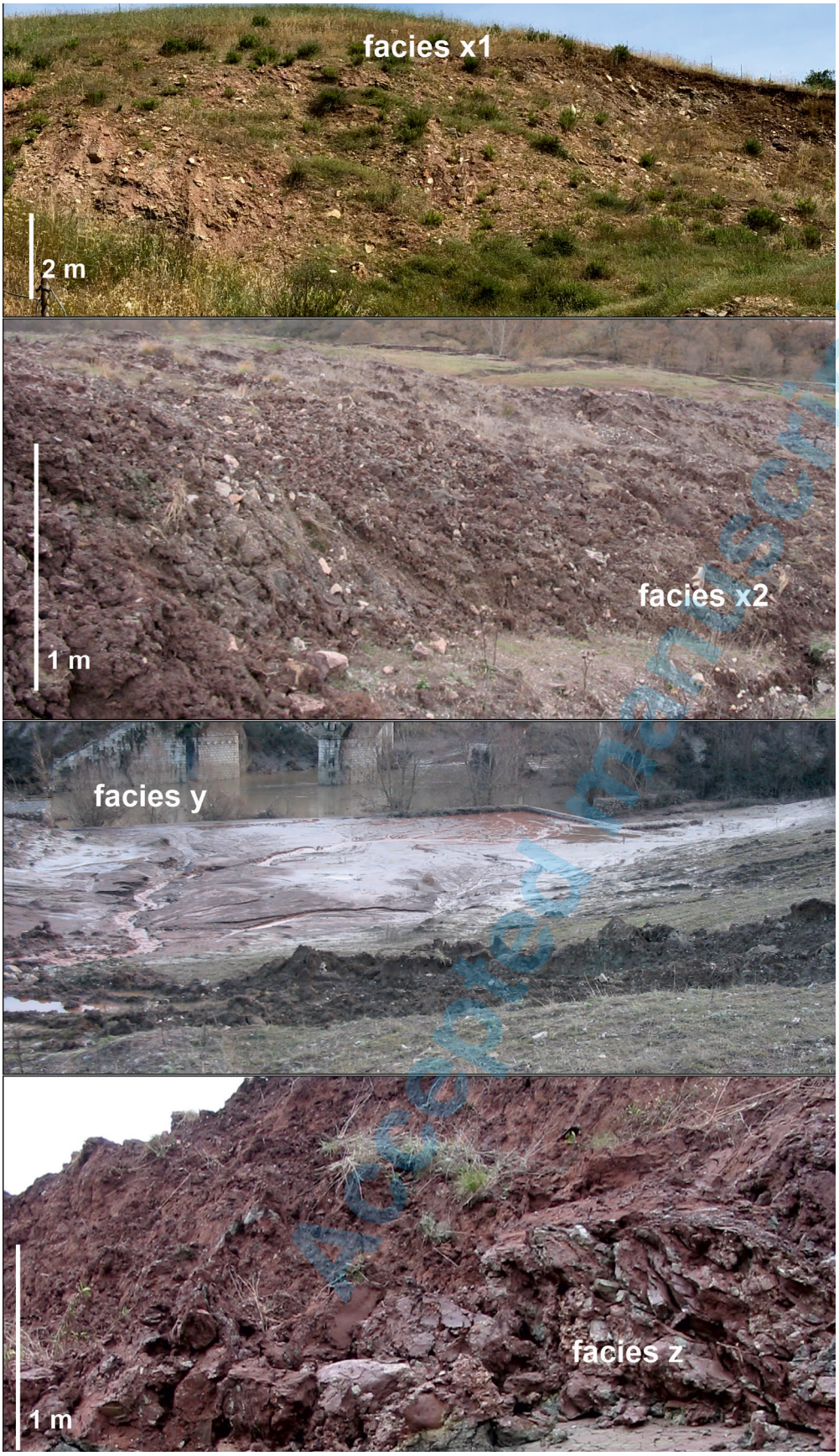




**Fig. 7 - Pictures showing the lithofacies x1, x2, z, and a mudflow event (facies y), as recognized within the landslide allostratigraphic units (UCN); for lithofacies descriptions see text.**

accumulation zone and several landslide bodies made of sediment slump (facies z) cropping out in the source area and along the left side of the valley. In the accumulation area, the $UCN_{a1bx2}$ landslide deposit shows several gravity-induced reverse shear planes. The $UCN_{a1c}$ (year 2015) and $UCN_{a1d}$ (year 2016) units groups a mud flow deposit (facies

y) in the BML channel and some landslide bodies in the source area (facies z). The facies y consists of laminated to massive grey-green clay, interpreted as suspension fall-out from a mud flow. Finally, the UCNa1e slump deposits detected in three landslide bodies of the source area took place in the years 2017-2018.

On the 2018 DTM (Fig. 2) we report a matrix-depleted blocky landslide in the source area and an incision channel that runs through the whole body of the landslide. In this channel the waterflow constantly reworks the debris, leaving limestone clasts in the channel bed and removing the mud which is carried away as suspended load. In the landslide accumulation zone, the lowermost water channel is reduced to a small incision driven by grooves traced by earthmoving vehicles.

## DISCUSSION AND CONCLUSIONS

In the past, the BML were mapped using out-of-date topographic maps and a scale inadequate for facing field work requirements (Servizio Geologico d'Italia, 2012; Cotecchia et al., 1986; Bentivenga et al., 2006, 2019). In these cases, both the landslide bodies and the bedrock were mapped in a roughly way and the ancient landslides were not mapped at all.

In our work, using two UAV-derived orthomosaic images and the extracted 1:1,000 scale topographic map, each landslide deposit of the BML were detected with regard to distinct activity episodes as well as the sedimentary bedrock was mapped with a greater lithological accuracy. This made it possible to create a very detailed map in which each landslide deposit is differentiated according to the time of activation. In addition, facies analysis of the landslide material and the distance of each body from its scarp allowed us to recognize the depositional processes and the related source area. Landslide mapping with eBee and data processing with Pix4D stressed that low-cost aerial vehicle can provide remote sensing at higher resolution able to represent the geomorphological variations through the time. This methodology, integrated with the classical geological field-survey methods, allowed increasing the precision and reliability of the final geological-geomorphological map. Regarding the bedrock, the number of mapped units (particularly within the Campomaggiore formation) and information about their lithological characteristics and deformation degree were widely increased.

The BML location and its evolution over time appear to be constrained by the geological context. Among the three $UCN_{a1}$, $UCN_{a2}$, and $UCN_{a3}$ landslide units, the oldest $UCN_{a3}$ (consisting of facies $x_1$ derived from the dismantling of the *Flysch Rosso*) is localized in the landslide feeding zone. The composition of the debris material (showing a strong affinity with the *Flysch Rosso*), facies analyses, and the landslide geometries, allowed us to attribute the landslide unit $UCN_{a2}$ to debris flows supplied by the *Flysch Rosso* outcropping at the highest elevations of the slope. This unit – however referred to the present-day erosion base-level because of its foot reached the thalweg of the major river – can be related to an activity older than 1973 (year of the modern BML activation; after Cotecchia et al., 1986). An unconformity (consisting of a deep U-shaped incision developed in the centre of the $UCN_{a2}$ landslide deposit) bounds the units $UCN_{a2}$ and $UCN_{a1}$. The 2014 to 2018 topographic data allowed mapping the $UCN_{a1}$ unit in terms of facies and depositional geometries, material composition, source area, and emplacement modes (see attached map). These younger events started with a high-magnitude debris flow occurred in 2014, that was followed by a period (2014-2018) of prevailing erosive processes. In this stage, the fine matrix of the oldest landslides was depleted by water flows in the feeding area, where small landslides (sediment slumps) also occurred. During the same stage, some mud flows ran along the incision channel, reaching the landslide foot. The composition of such flows indicates the Campomaggiore formation as their prevalent source area.

## ACKNOWLEDGEMENTS

We wish to thank two anonymous referees and the Associate Editor Marta Della Seta for their accurate revision. English text revised by the Centro Linguistico di Ateneo of the Basilicata University. This research has been supported by MIUR PON R&I 2014-2020 Program (project MITIGO, ARS01_00964).

## REFERENCES

Bentivenga M., Giocoli A., Palladino G, Perrone A., Piscitelli S. (2019) - Geological and geophysical characterization of the Brindisi di Montagna Scalo landslide (Basilicata, Southern Italy). Geomatics, Natural Hazards and Risk, 10, 1367-1388.

Bentivenga M., Grimaldi S., Palladino G. (2006) - Caratteri geomorfologici della instabilità del versante sinistro del fiume Basento interessato dalla grande frana di Brindisi di Montagna Scalo (Potenza, Basilicata). Giornale di Geologia Applicata, 4, 123-130.

Chang K.H. (1975) - Unconformity-bounded stratigraphic units. Geol. Soc. Am. Bull., 86, 1544-1552.

Clapuyt F., Vanacker V., Oost K.V. (2016) - Reproducibility of UAV-based earth topography reconstructions based on structure-from-motion algorithms. Geomorphology, 260, 4-15.

Cocco E., Cravero E., Ortolani F., Pescatore T., Russo M., Sgrosso I., Torre M. (1972) - Les facies sedimentaires du Basin Irpinien (Italie Meridionale). Atti dell'Accademia Pontaniana, Napoli, 21, 1-13.

Cotecchia V., Del Prete M., Federico A., Fenelli G.B., Pellegrino A., Picarelli L. (1986) - Studio di una colata in formazioni strutturalmente complesse presso Brindisi di Montagna Scalo (PZ). Atti del XVI Conv. Naz. Geotecnica (A.G.I.), 14-16 maggio, Bologna, 253-264.

Cruden D.M., Varnes D.J. (1986) - Landslide types and processes. In: Turner AR and Schuster RL, editors. Landslides: Investigation and mitigation. Sp. Rep. 247, Transportation Research Board, National Research Council, National Academy Press, Washington DC, 36-72.

Giannandrea P., Loiacono F., Maiorano P., Lirer F., Puglisi D. (2016) - Geological map of the eastern sector of the Gorgoglione Basin (southern Italy). Ital. J. Geosci., 135(1); including a geological map at 1:25,000 scale. LAC, Firenze.

Guerriero L., Di Martire D., Calcaterra D., Francioni M. (2020) - Digital Image Correlation of Google Earth Images for Earth's Surface Displacement Estimation. Remote Sensing, 12, 3518.

Hedberg H.D. (1976) - International Stratigraphic Guide, Wiley and Sons, New York, 200 pp.

Mazzanti P., Caporossi P., Muzi R. (2020) - Sliding Time Master Digital Image Correlation Analyses of CubeSat Images for landslide Monitoring: The Rattlesnake Hills Landslide (USA). Remote Sensing, 12, 592.

North America Commission on Stratigraphic Nomenclature (1983) - North America stratigraphic code. Am. Ass. Petrol. Geoll. Bull., 67, 841-875.

Patacca E., Sartori R., Scandone P. (1990) - Tyrrhenian basin and Apenninic arc: kinematic relations since Late Tortonian times. Mem. Soc. Geol. It., 45, 425-451.

Pescatore T. (1978) - Evoluzione tettonica del Bacino Irpino (Italia meridionale) durante il Miocene. Boll. Soc. Geol. It., 97, 783-805.

Pescatore T., Renda P., Schiattarella M., Tramutoli M. (1999) - Stratigraphic and structural relationships between Meso-Cenozoic Lagonegro basin and coeval carbonate platforms in southern Apennines, Italy. Tectonophysics, 315, 269-286.

Pescatore T., Sgrosso I., Torre M. (1971) – Lineamenti di tettonica e sedimentazione nel Miocene dell'Appennino campano-lucano. Mem. Soc. Natur. in Napoli, I (Parte seconda): 337-406 – suppl. al vol. 80 (1971) del Boll. Soc. dei Natural. in Napoli.

Sabato L., Gallicchio S., Pieri P., Salvini G., Scotti P., (2007) - Cretaceous anoxic events in the argilliti e radiolariti di Campomaggiore unit (Lagonegro-Molise basin, southern Italy). Boll. Soc. Geol. It., Spec. Issue 7, 57-74.

Salvador A. (1987) - Unconformity-bounded stratigraphic units. Geological Society American Bulletin, 98, 232-237.

Salvador A. (ed.) (1994) - International stratigraphic guide. International Union of Geological Sciences, Trondheim, Norway, and Geological Society of America, Boulder, 214 pp.

Scandone P. (1972) - Studi di geologia lucana: Carta dei terreni della serie calcareo-silico-marnosa e note illustrative. Boll. Soc. Natur. in Napoli, 81, 225-300.

Schiattarella M., Giannandrea P., Principe C., La Volpe L. (2016) - Note Illustrative della Carta Geologica d'Italia alla scala 1:50.000, – F. 451 Melfi. 141 pp. Litografia Artistica Cartografica, Firenze.

Scrocca D. (2010) - Southern Apennines: structural setting and tectonic evolution. In: Beltrando M., Peccerillo A., Mattei M., Conticelli S., Doglioni C. (Eds.), The Geology of Italy. Journal of the Virtual Explorer, Electronic Edition, 36, paper 13.

Servizio Geologico d'Italia (2012) - Carta Geologica d'Italia alla scala 1:50.000, F. 470 Potenza. ISPRA, Roma. Spilotro G., Canora F., Pellicani R., Vitelli F. (2016) -Risk and mitigation of the large landslide of Brindisi di Montagna. In: Lollino G, Giordan D, Thuro K, Carranza-Torres C, Wu F, Marinos P, Delgado C, (eds.). Engineering Geology for Society and Territory. Cham, Springer, 1-6.

Stumpf A., Malet J.P., Delacourt C. (2017) - Correlation of satellite image time-series for the detection and monitoring of slow-moving landslides. Remote. Sens. Environ, 189, 40-55.

Turner D., Lucieer A., de Jong S. M. (2015) - Time series analysis of landslide dynamics using an unmanned aerial vehicle (UAV). Remote Sensing, 7, 1736-1757.

*Manuscript received 1 August 2022; accepted 27 January 2023; published online XX April 2023;*
*editorial responsibility and handling by M. Della Seta.*